AIAA AVIATION Forum
13-17 June 2016, Washington, D.C.
16th AIAA Aviation Technology, Integration, and Operations Conference

10.2514/6.2016-3744

Conceptualizing Active Load Alleviation: Impacts on Transport Category Aircraft Wing Structural Design

Mathew R. Allyn[1] and Timothy T. Takahashi[2]
Arizona State University, Tempe, AZ, 85282

This paper examines the structural effects of applying active-load-alleviation, through a symmetric negative incidence of the ailerons, to the detailed structural design of the torque box of a commercial aircraft. We will examine this effect across three different configurations, representing: 1) a regional jet (50,000-lbm), 2) a small narrow-body aircraft (100,000-lbm), and 3) a large narrow-body aircraft (150,000-lbm). We modelled the aerodynamic effects of active aileron reflex using a vortex lattice CFD code. Both baseline, elliptical, and reflexed aileron loads drove an iterative wing primary structure sizing tool that considers both the strength and the buckling stability of structure. We found that active-load-alleviation consistently leads to lighter structures through a reduction in bending moment. Because these structures are buckling rather than strength limited, we found that active-load-alleviation may not yield as much weight savings as its implied reduction in root bending moment might otherwise indicate.

Nomenclature

BL	=	Butt Line (ft)
WL	=	Water Line (ft)
α	=	Angle of Attack (°)
CL	=	Coefficient of Lift
t/c_{root}	=	Thickness to Chord Ratio of Wing Section at the Root of the Wing (%)
t/c_{tip}	=	Thickness to Chord Ratio of Wing Section at the Tip of the Wing (%)
b	=	Span of Wing (tip-to-tip) (ft)
c	=	Chord of Wing (ft)
TR	=	Taper Ratio (ratio of tip-chord to root-chord)
Sref	=	Wing Planform Area (ft^2)
MTOW	=	Maximum Takeoff Weight (lbm)
MLW	=	Maximum Landing Weight (lbm)
$\pm Nz$	=	Load factor in the WL direction (g's)
σ_{ty}	=	Material Tension Yield Strength (lbf/in^2)
σ_{cy}	=	Material Compressive Yield Strength (lbf/in^2)
σ_{su}	=	Material Ultimate Shear Strength (lbf/in^2)
ρ	=	Material Density (lbf/in^3)
E	=	Material Elastic Modulus (lbf/in^2)
F.O.S.	=	Factor of Safety

[1] M.S. Candidate, Aerospace and Mechanical Engineering, School of Engineering for Matter, Transport & Energy, P.O. Box 876106, Tempe, AZ. Student Member AIAA.
[2] Professor of Practice, Aerospace and Mechanical Engineering, School of Engineering for Matter, Transport & Energy, P.O. Box 876106, Tempe, AZ. Associate Fellow AIAA

I. Introduction

AIRCRAFT wing design is a complicated endeavor that requires the delicate balance of factors such as weight of the wing, structural strength, structural stiffness and aerodynamic performance. The perfect balance of these factors is arguably the most important factor in the overall aircraft design, since it will determine the success or failure of an aircraft design.

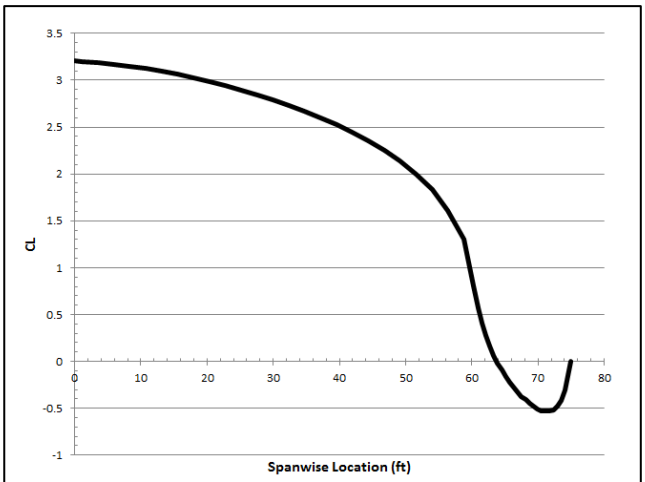

Figure 1. Sample Active-load-alleviation Lift Distribution.

For traditional aerodynamically oriented wing design, engineers seek to obtain an elliptical lift distribution across the wingspan. The idea behind this is that this will allow for the maximum lift possible across the wing while minimizing the induced drag formed as a byproduct of lift. Conversely, the wing can be designed to have an aerodynamically inferior transverse lift distribution that has a lower in-flight bending moment. The elliptical transverse load design philosophy may be great for aircraft performance, but it can create problems in terms of structural design because the wing needs to be highly stressed for ultimate load situations that include maneuvering flight. For example, a "triangular" transverse load design philosophy might produce a lighter weight structure, but such a design saddles the aircraft with increased induced drag (and hence higher fuel consumption) throughout its life. In order to attain the best of both worlds, we can design wings that adapt to flight conditions. At nominal cruise conditions, they develop the aerodynamically ideal elliptical span load. During maneuvering flight, they can actively deflect ailerons upwards to reduce the overall aerodynamic bending moment. An example of what this lift distribution would look like is pictured in Figure 1.

Disney [1] documented an industry example of how active-load-alleviation can improve the structural performance of an aircraft in regards to the C-5A program. In this paper, he found that with a modification to the aircraft allowing for active control of the ailerons, peak wing stresses could be reduced locally by as much as 27%. This can materially improve the fatigue life on such an airframe.

Xu [2] also explores active-load-alleviation and its relationship to natural laminar flow. In this work, he found that active-load-alleviation could be used to reduce some of the structural penalties and thus create thinner wings with a higher aspect ratio. This would then theoretically translate fuel and cost savings on the part of each aircraft.

II. Analysis Tools

The method used to model and examine the active-load-alleviation affect begins with deriving a lift distribution model across the half span of the wing using the tool discussed in subsection A. Then the information outlined in Table 3, and the selected lift distribution was inputted into the structural sizing tool which then calculated a wing size estimation solution.

A. Aerodynamic Loads

We used VORLAX, a NASA / Lockheed vortex lattice method code, to determine the lift distributions of the elliptical and load alleviated lift distributions [3]. VORLAX, known to be accurate under attached flow conditions, can be used to predict the aircraft stability, pressure distribution, drag coefficient, and span wise lift

Figure 2. VORLAX Wing Model. *Note the numbers refer to each reference station, located at the end of each respective panel. Panel numbering starts at the inboard portion and continues spanwise.*

distribution of aero structures.

VORLAX requires the user to input Mach numbers, angles of attack, and sideslip angles for each desired solution. In VORLAX, the aerodynamic shape is defined by a collection of panels of given dimensions. Each panel may have its twist (local incidence), camber, and thickness profile modelled.

To derive a general lift distribution, we configured VORLAX with a notional three panel wing, as shown in figure 2. To simplify the formulation, we did not model a fuselage, or wing mounted engines. Neither did we add camber nor thickness profiles to this model. The wing was input into VORLAX such that panel 1 comprises the majority of the wing, panel 2 is the portion of the wing in front of an outboard aileron and panel 3 is the aileron itself. Note that leading edge suction in front of the aileron was turned off, so that it would simulate the aileron being directly attached to the wing.

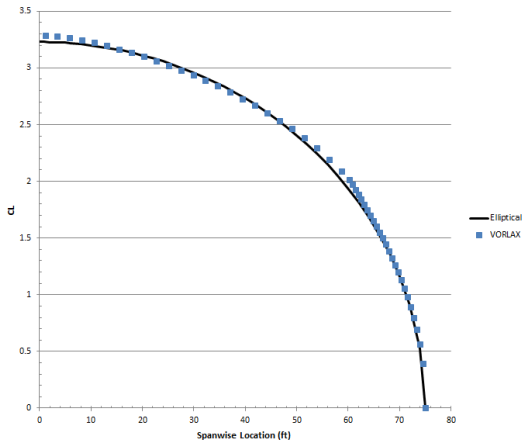

Figure 3. VORLAX Elliptical Lift Distribution.

We analyzed this wing in VORLAX at Mach of 0.74 and at α of 2°. In order to develop an elliptical lift distribution, we varied the twist of the panels to final values as shown below in Table 1 and Figure 3. We assume here that the spanwise shape of the reflexed aileron lift distribution is generally representative of wings designed to any subsonic Mach number and reasonable lift coefficient.

Table 1. VORLAX Inputs.

Station	1	2	3
Twist (°)	0.086	-0.487	-1.146

Once the elliptical case was found, the aileron panel was successively deflected upwards to find the deflection where the wing was essentially unloaded (zero section CL) at the wing tip. From Figure 4, the 2.5° case of aileron reflex was selected as the profile for future steps.

B. Inertial Loads

In order to provide the structural sizing model some level of inertial relief, we modelled the wing to include a distributed inertial load to represent full fuel tanks. But to further simplify the estimation, it was assumed that the engines were placed on the fuselage, and as a result not added as inertial relief.

C. Structural Sizing Tool

To design the wing structure we must first identify the outer-mould-line loft and the design loading cases. This method, developed by Takahashi & Lemonds [4][5], is summarized here.

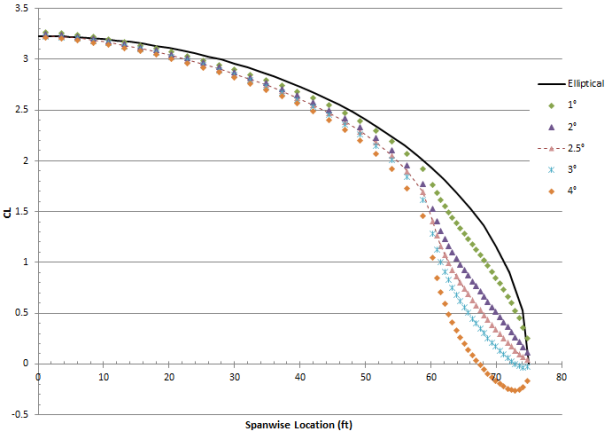

Figure 4. VORLAX Lift Distribution with Aileron Twist. *Each data set refers to the degree of negative α given to the aileron. The same elliptical curve from figure 3 is left in figure 4 for reference.*

We size the wing structure to a series of flight loading cases. These include: 1) flight loads based upon a maximum flight weight, *MTOW*, and a design load factor in terms of positive (NZ_{max}) and negative (NZ_{min}) g forces and 2) ground loads based upon a maximum landing weight, *MLW*, and a negative (NZ_{min}) g force applied at the landing gear frame ribs. Flight envelope load factors are specified by the FAA in 14 CFR § 25.337. Since we study larger transport aircraft, *Nzmax* = +2.5g for flight. Nzmin = -3.0g to represent a hard landing.

Material properties are given by the sorts of properties found in MIL HDBK-5J [6]. In other words, isotropic properties representing bulk characteristics including the tensile yield strength (σ_{ty}), compressive yield strength (σ_{cy}), ultimate shear strength (σ_{su}), elastic modulus (E) and density (ρ). These properties may be derated as necessary by the statutory factor-of-safety (FOS) given by the FAA in 14 CFR § 25.303 (typically 1.5). Thus the derated material characteristics are:

$$\sigma_{ty\_derated} = \sigma_{ty}/FOS \quad (1)$$
$$\sigma_{cy\_derated} = \sigma_{cy}/FOS \quad (2)$$
$$\sigma_{su\_derated} = \sigma_{su}/FOS \quad (3)$$

In this study, we assume that the structure will be made from Al 2024-T4, and as such the material properties used are listed below in Table 2

Table 2. Material Properties.

σ_{ty}	72,000 lbf/in^2
σ_{cy}	70,000 lbf/in^2
σ_{su}	45,000 lbf/in^2
E	1.07E+07 lbf/in^2
ρ	0.1 lbm/in^3
F.O.S.	1.5

We define the wing planform as a modified trapezoid upon which reference values are computed (see Figure 5). Engineers specify the basic planform in terms of: 1) the wing-tip to wing-tip overall span (b), 2) its basic trapezoidal taper ratio (TR) which is defined as the ratio of tip to root chord of the basic trapezoid, 3) its mid-chord sweep ($\Lambda_{c/2}$) angle of the basic trapezoid as well as 4) an arbitrary spanwise chord function ($c(y)$) which permits yehudis (chord-wise extension at the wing/fuselage junction), raked wingtips and other non-trapezoidal changes to the wing planform. Similarly, the overall wing thickness is defined in terms of an arbitrary spanwise wind referenced thickness to chord ratio ($t/c(y)$); see Figure 6.

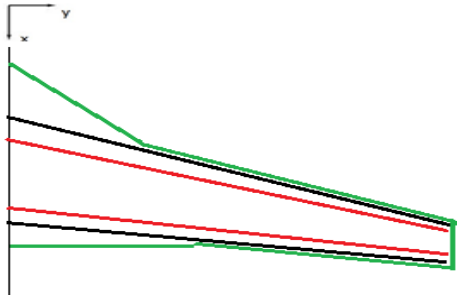

Figure 5. *Sketch of the trapezoidal basis for wing spar locations superimposed upon an arbitrary cranked planform. The arbitrary planform is shown in green, the fundamental trapezoidal geometry is shown in black, the spar locations are shown in red.*

Thus, the actual maximum thickness of the wing section may be defined in terms of the arbitrary functions $(t/c)(y)$ and $c(y)$ as:

$$t(y) = \left(\frac{t}{c}\right)(y) * c(y) \quad (4)$$

Whereas the spar locations are predicated on a spanwise invariant percentage chord location based upon the fundamental trapezoidal planform. Typically the front spar is located at the 15% chord point;

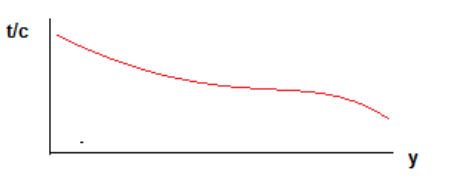

Figure 6. *Sketch of spanwise variation in wing thickness to chord ratio (t/c).*

the rear spar at the 65% chord point. Thus, the distance between the spars is:

$$dist_{betweenspars}(y) = 0.5\, c(y) \quad (5)$$

From this geometry (depicted in Figure 7), the reference area (*Sref*) and aspect ratio (*AR*) may be defined as follows, where:

$$Sref = b \cdot \bar{c} \quad (6)$$
$$AR = b/\bar{c} \quad (7)$$
$$TR = c_{tip}/c_{root} \quad (8)$$

and

$$\bar{c} = 1/2(c_{tip} + c_{root}) \quad (9)$$

Refer again to Figure 7. This formulation allows us to represent the wing in terms of a local coordinate system oriented with the mid chord sweep. In this system, the structural semi-span of the wing (that aligned with the *y'* coordinate axis) is defined as:

$$(\tfrac{b}{2})_{structural} = (\tfrac{b}{2})/\cos(\Lambda_{c/2}) \quad (10)$$

In addition to specifying the location of the front and rear spars, we may define the rib-to-rib spacing of the wing primary structure in terms of a spanwise distance, Δy; these too may be seen in Figure 8. Thus, the presence of wing sweep alters the length of unsupported panels in the structural, *y'*, axis:

$$\Delta y' = \Delta y/\cos(\Lambda_{c/2}) \quad (11)$$

A real wing will have finite weight, which will provide inertial relief against lift induced shear and bending moment. To determine design loadings the weight of the wing must be taken into account.

The weight distribution consists of

- basic wing structure
- power plants
- landing gear, if mounted on the wing,
- other heavy items (i.e. fuel, flap actuators, flaps, ailerons)

At in flight conditions (positive *Nz* operation), fuel and engine weight is a relieving load. Thus, a considerable structural savings may result from the reduction in loading. However, in a hard landing these lumped and distributed weights work against the designer (see Figure 8).

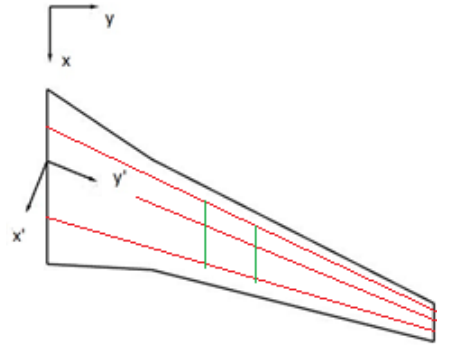

Figure 7. *Sketch of the mid-chord-sweep aligned structural coordinate system (x' – y') as opposed to the global lofting coordinate system (x – y). Spar and stiffeners are called out in **red**. Rib locations are called out in green.*

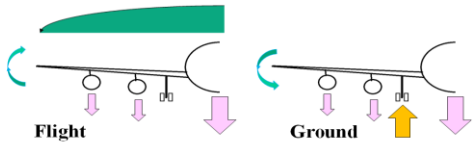

Figure 8. *Sketch of the shear and bending moment arising from wing structural and non-structural mass under flight and hard-landing loading conditions.*

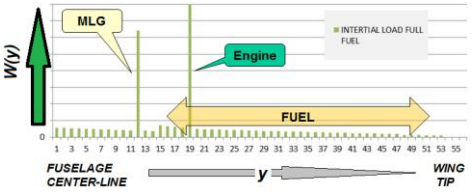

Figure 9. *Sketch of a "lumped mass" model comprising wing structural and non-structural mass under a nominal 1-g loading.*

We use a lumped mass approach to allocate the weight of the wing for further analysis. Wing weight is distributed across the span as discretized continuous loads (a smeared representation of the weight of flaps, leading edges, fuel and a primary structure) plus discrete point loads (representing engines, pylons, the landing gear, etc.). Together they define a weight distribution, *W(y)*; see Figure 9.

To render a physics-based method computationally tractable, we specify an analytical transverse aerodynamic load distribution:

$$L'(y) = C_L(y) q\, c(y) \tag{12}$$

Where $C_L(y)$ represents the section lift coefficient, C_L, as a function of the butt-line, y.

From this, the integrated load of the wing can be found by integrating this function from wing-tip to wing-tip:

$$L = \int_{-b/2}^{+b/2} L'(y)dy \tag{13}$$

Recall that from a structural design standpoint, the global lofting coordinates (x,y,z) are less applicable. It is better, if we are to consider the wing as some form of equivalent beam, aligned with axis of structural sweep, to compute shear and bending moment in terms of the transformed coordinate system, x',y',z'. Thus, the relevant shear and bending moment functions arising purely from aerodynamic loads are of the form:

$$\tau'(y') = \int_{y'}^{(\frac{b}{2})/\cos(\Lambda_c)} Nz\left(L'(\tilde{y}') - W'(\tilde{y}')\right)d\tilde{y}' \tag{14}$$

and

$$M'(y') = \int_{y'}^{(\frac{b}{2})/\cos(\Lambda_c)} \tau'(\tilde{y}')d\tilde{y}' \tag{15}$$

Where for purposes of simplification, $L'(y')$ is the 1-g flight load distribution at the design loading condition, $W'(y')$ is the 1-g weight distribution at the design loading condition, and Nz is the design load factor. The three most important envelope load cases comprise: 1) a maneuver at positive, *Nzmax*, (typically *Nzmax=2.5-g's*) at maximum take-off-weight, *MTOW*, with the maximum payload and the least favorable (minimum and inboard weighted) fuel loading in the wing, 2) a maneuver at negative, *Nzmin*, (typically *Nzmin=-1-g*) at maximum take-off-weight, *MTOW*, with a minimum payload and a full fuel load in the wing, and 3) a hard-landing at *Nz=-3-g's*, at maximum landing weight, *MLW*, with a minimum payload and the greatest possible fuel load in the wing. Each case stresses the wing structure to the sort of worst case loading event the aircraft is likely to encounter in operation. Because positive flight design load factors are always higher than for negative flight design load factors, the limiting flight loads occur where wing tips bend up. Thus, the wing upper surface is usually critical for compression loads while the wing lower surface sees peak tension loads. Alternatively, under a hard landing condition, the wing tips bend down. The wing lower surface sees critical compression loads. The wing upper surface sees peak tension loads. (see Figure 10)

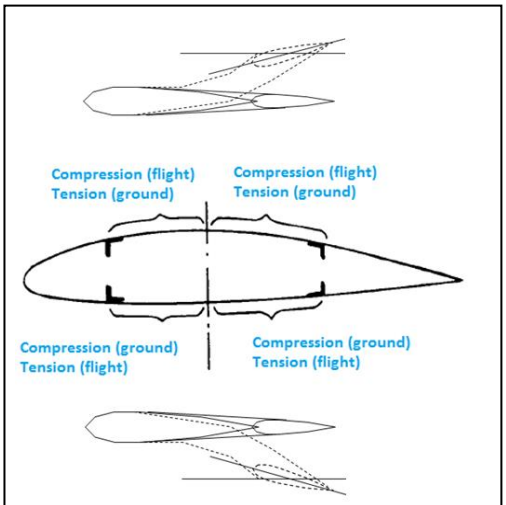

Figure 10. *Sketch describing "envelope" loading situations (+Nz flight vs. –Nz ground).*

The wing's torque box (comprising the upper and lower surface skins, spar caps and spar webs) must resist all imposed moments (both the transverse bending moment and torsional moments resulting directly from wing camber or indirectly from wing sweep). Wings experience aerodynamic forces normal to the local orientation of the wing, rather than forces directly opposing weight. Because a transversely loaded swept wing (without any torsional loading from wing camber) still develops an overall pitching moment about the wing-body-root, the indirect, wing

sweep induced torsion cannot be neglected. Thus, a simplified root-bending-moment formulation (even one including the structural span) does not fully capture the structural design challenge.

While we computed in-plane (y' reference axis) bending moments, the net bending torque distribution comprising secondary bending torque components induced indirectly as a result of sweep is:

$$T'(y') = \int_{y'}^{(\frac{b}{2})/\cos(\Lambda_{\frac{c}{2}})} \tau'(\tilde{y}')\sqrt{(1+\sin(\Lambda_{c/2})^2)}d\tilde{y}' \quad (16)$$

Note that for an unswept wing ($\Lambda=0^o$), the net in-plane bending torques are identically equal to the transverse bending moment of the wing.

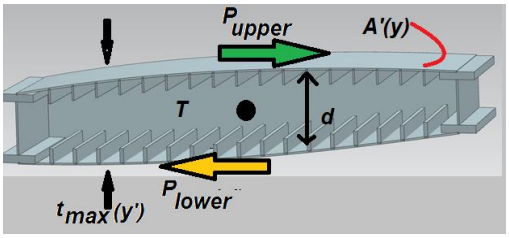

Figure 11. *Sketch resolving wing bending moment into forces along the upper and lower wing covers (comprising the spar caps, skin and any stiffeners).*

Neglecting buckling concerns, the wing torque box must locally and globally withstand all aerodynamically applied torques without yielding in tension or compression. This provides a means to determine the lower bound, the minimum cross sectional area of the upper or lower covers. If, for buckling reasons, additional material is needed, the stiffened panel will be heavier than needed to resist simple tension loading.

In our computational application, applied forces and moments were computed at discrete spanwise stations, *i*, representing the unsupported wing section between two adjacent chordwise ribs. Our nomenclature locates *Wing Station 1* along the fuselage centerline, and *Wing Station n* at the wing tip.

Any given bending moment (or torque) can be resolved into an individual force couple, of equal and opposite forces, *P*, acting over a distance, *d*. (refer to Figure 11)

$$T = P\,d \quad (17)$$

For a typical wing, comprising a NACA 4-digit thickness form with the front spars located at 15% chord and the rear spar located at the 65% chord point; the "average" distance between upper and lower wing covers is only 70% of the magnitude of the maximum thickness of the wing. Thus, the tension and compression forces in respective lower and upper wing covers are equal to the torque divided by 0.70 of the local wing section thickness:

$$P = \frac{T}{d} \xrightarrow{yields} P(y') = +/- \frac{T(y')}{0.70\,t(y')} \quad (18)$$

As shown in Figure 10, above, for positive *Nz* cases, the wing lower cover will be in tension and the wing upper cover will be in compression. The opposite holds true for negative *Nz* cases. The wing lower cover will be in compression; the wing upper cover will be in tension.

Thus, for a given material yield strength, σ_{ty}, the structure can withstand a tensile force proportional to the material area in upper and lower covers. Thus, the tensile strength limited cross-sectional area, *A*, of the upper or lower covers (sliced in a chord-wise plane) is:

$$A_{upper\_and\_lower\_cover} \geq P(y')/\sigma_{ty} \quad (19)$$

Substituting equation 4.45 into 4.46 results in the following relationship:

$$A_{upper\_and\_lower\_cover} \geq T(y')/(0.70\,t(y')\,\sigma_{ty}) \quad (20)$$

The relevant torque box area, $A_{upper\_and\_lower\_cover}$, for this computation comprises the following "bending resistant material." The lower bound of this inequality represents the amount of material needed for a purely

"Strength Based" design. Refer to Figure 12, overleaf. The spar usually looks like a modified "I" beam where the vertical stroke of the "I" is the spar web (typically quite thin) and the top and bottom strokes of the "I" the spar caps. Thus, when the wing resists transverse bending the spar caps and skin carry the majority of the stresses (as opposed to the spar webs) because the spar caps are furthest from the shear center of the equivalent beam.

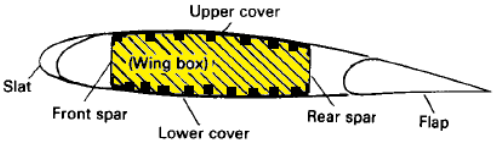

Figure 12. *Sketch resolving the torque box into spar caps, skin and any stiffeners.*

In order to develop the complete torque box geometry (that is to size the spar web, spar caps, skins and stiffeners) we must balance loads between spar caps, skins and main spar. Our algorithm will ensure that we do not violate five important constraints:

- The ensemble will not exceed the tensile yield strength of the material on tension surfaces
- The ensemble will not exceed the compressive buckling strength of the geometry on compression side stiffened panels
- Individual strips bounded by chord-wise stiffeners and span-wise ribs will not buckle in compression
- The spar web will sustain applicable wing shear forces without exceeding material shear strength limits
- The rib webs will sustain applicable wing shear forces without exceeding material shear strength limits

This method makes certain assumptions (static determinacy is approximated by crippling factors to make up for some static indeterminacy in the built-up structure), but is computationally tractable.

To size the wing structure on a bay-by-bay basis, we must size the following elements, based upon the aforementioned constraints.

- The upper cover (skin and stiffeners) will be sized for tensile strength from ground loads and compressive stability (buckling) from flight loads
- The lower cover (skin and stiffeners) will be sized for tensile strength from flight loads and compressive stability (buckling) from ground loads
- The spar caps will be sized based upon tensile strength from ground loads traded against the overall compressive strength and structural stability required by flight loads (the spar cap sizing can be traded off against the number and size of stiffeners)
- The spar web is sized for tensile and compressive strength resisting primary wing bending as well as fuel slosh / crash loads

To determine the optimum sizing, we developed an algorithm that grew the wing from root to tip. For each bay (comprising the area between two neighboring ribs), the algorithm enumerates all possible combinations of upper cover geometry, lower cover geometry and spar geometry. For each possible design, we compute the relevant critical loading conditions and compare these against our estimated loads. From this collection of possibilities, the algorithm selects the minimum weight configuration that satisfies all feasibility criteria.

We found it useful to specify the rib-to-rib spacing distance as well as a stringer-to-stringer spacing distance as independent design variables that remain constant over the entire wing. For these wings, we let the computer to enumerate 34 discrete possible spar cap sizes (from 1-inch wide by ¼-inch thick to 10-inches wide by 3-inches thick), 40 discrete possible skin thicknesses (from 18 gauge aluminum through 1-inch) and 21 discrete stringer geometries (from 1x skin-thickness wide by 2x skin-thickness tall to 2x skin-thickness wide by 8x skin-thickness tall). From this enumerated set of 24,000 possibilities (per bay) we then dismiss all geometries whereby the overall cross-sectional-area of the implied geometry is less than $A_{upper\_and\_lower\_covers}$ as governed by equation 19.

We assume that the stiffened skin panels are statically determinate; they share a fraction of the total load proportional to their respective cross-sectional areas. From this, we can infer from the compression load as applied

to the entire stiffened panel, component compression loads as applied to individual spar caps, the skin, an individual stringer or to the unsupported strip of skin between two stiffeners.

Niu [7] provides a stiffened panel buckling equation:

$$P_{cr\_stiffened\_panel} = \pi^2 \, E \, \left(\frac{\rho^2}{L^2}\right) A_{stiffenedpanel} \tag{21}$$

where

$$A_{stiffenedpanel} = thickness_{skin} \, dist_{spartospar} + \#_{stringers}(height_{stringer} \, thickness_{stringer}) \tag{22}$$
$$L = dist_{ribtorib} \tag{4.50}$$

The radius of gyration, ρ, is described by:

$$\rho^2 = (b^2 \left(\frac{d}{b}\right)^3 \left(\frac{Ts}{t}\right))/(12 \left(1 + \left(\frac{d}{b}\right)\left(\frac{Ts}{t}\right)^2\right)\left(4 + \left(\frac{d}{b}\right)\left(\frac{Ts}{t}\right)\right)^2 \tag{23}$$

with the following relationships:

$$b = dist_{spartospar}/(\#_{stringers} + 1) \tag{24}$$
$$d = height_{stringer} \tag{25}$$
$$Ts = thickness_{stringer} \tag{26}$$
$$t = thickness_{skin} \tag{27}$$

Niu recommends another equation to estimate the maximum load the unsupported skin can sustain without buckling.[6] He employs the Euler buckling equation using NASA factors for a strip where all edges are effectively clamped and fully supported.

$$P_{cr\_strip} = 6.3 \, E \, \left(\frac{t^3 W}{b^2}\right) \tag{28}$$

where

$$W = dist_{spartospar}/(\#_{stringers} + 1) \tag{29}$$
$$t = thickness_{skin} \tag{30}$$
$$b = dist_{ribtorib} \tag{31}$$

If these critical value, *Pcr_stiffenedpanel* or *Pcr_strip*, exceeds 150% of the actual compression force applied to the stiffened skin, the algorithm deems the proposed design infeasible. It will move on, and examine other enumerated possibilities. This algorithm can find designs that simultaneously satisfy compression yield, tension yield, stiffened panel buckling and local strip buckling constraints.

In order to size spar webs and rib webs for the shear loading condition, recall that the peak shear stress in a thin plate is:

$$\sigma_{s\_max} = 1.5 \, (\frac{\tau}{b \, h}) \tag{32}$$

where, τ is the applied shear, *b* is the web thickness and *h* is the physical height of the plate.

Spar webs must support shear generated by the aero loads of the wing. Because a multi-spar wing is a statically indeterminate structure, the load sharing between spars is not clearly defined. Industry practice may assume that

each spar could be responsible to momentarily sustain the entire shear load. Thus, the spar web thickness for any given bay is proportional to the peak shear force that the wing must resist and inversely proportional to the height of the aft spar web. On a typical NACA 4-digit airfoil section, the maximum thickness point on the form is found around the 30% chord point; the front spar height is 80% of the maximum section thickness. The more critical rear spar height is typically only 60% of the magnitude of the maximum thickness of the wing. Thus, the rear spar height controls the spar web thickness:

$$thickness_{sparweb}(y') = 1.5\frac{\tau(y')}{(0.6\,t(y'))\sigma_{su}} \tag{33}$$

where $t(y') = (t/c)(y')\,c(y)$ and σ_{su} is the derated maximum allowable shear strength of the material.

Rib webs must tie the upper and lower covers together. Shear forces of the web are driven by the net loads across wings top and bottom.

$$thickness_{rib_{web}}(y') = 1.5\frac{\tau(y')}{\left(0.6\,dist_{betweenspars}(y')\right)\sigma_{su}} \tag{34}$$

Following this procedure, our algorithm develops the minimum weight torque box geometry (sizing the spar web, spar caps, skins and stiffeners, requires us to balance loads between spar caps, skins and main spar) of a feasible wing. Our final, coded optimization algorithm also includes some heuristics to keep the size of structural elements from oscillating from one bay to the next.

We used the normalized lift distribution data collected in VORLAX to determine the lift value for each cell (structural bay) in the structure sizing tool. The sizing tool did this by comparing the location of the desired cell with the locations for the lift distribution values and choosing the closest value for use. Thus, we can compare wings designed to the purely elliptical lift distribution against wings designed with reflexed ailerons that unload the wingtips.

III. Trade Studies and Results

Our trade studies examine the effects of applying this technology to a variety of airframes. The aircraft dimensions for the regional, small narrow body, and large narrow body are loosely based on dimensions for the Canadair CRJ-200, Boeing 737-100, and Airbus A320-200 respectively. We would hope to see, in each case, that the incorporation of active-load-alleviation will develop a lighter weight wing structure.

Table 3. Test Aircraft Dimensions.

Category	*Regional (50,000 lbm)*	*Small Narrow Body (100,000 lbm)*	*Large Narrow Body (150,000 lbm)*
Inputted MTOW (lbm)	51,000	111,000	172,000
MLW (lbm)	40,800	88,800	137,600
Span (ft)	69.5	93	111.25
Sref (ft^2)	587	980	1318
Sweep (°)	24.5	25	25
t/c_{root}	0.132	0.154	0.1515
t/c_{tip}	0.1	0.108	0.1084
TR	0.259	0.213	0.24

The actual torque box weight results from our trade studies are presented in Figure 13. In each case the rib-to-rib spacing and stiffener spacing inside the structure of the wing were varied from 12 inches to 20 inches, and 3 to 4 inches respectively. Note that Figure 13 was used to select the ideal design that created the lightest actual torque box weight case for each category of aircraft.

Figure 13a displays one of the most striking results where the addition of active-load-alleviation noticeably causes a general reduction in the majority of torque box weights calculated, except for a few cases that had weights in the non-load alleviated range. Also when the non-load alleviated case and load alleviated cases are compared a trend related to the rib-to-rib spacing emerges; where the shorter the length of the rib-to-rib spacing appears to cause a definite "sweet spot" for producing the lightest weight torque box regardless of the amount of active-load-alleviation.

In Figures 13b and 13c we see two notable behaviors; the first being that the increase in stiffener spacing seems to lead to the production of lower weight design points than the previous, shorter spacing. But this behavior is not guaranteed for all points in each case where it can be seen that certain rib-to-rib spacing values will create a comparably heavier weights than lighter. Additionally, we see that the use of active-load-alleviation seems to create more variation in weight for each respective stiffener spacing. This then ties into the second notable behavior, being that the addition of active-load-alleviation does not create the general shift seen in the regional jet case. Instead, the addition of active-load-alleviation appears to be beneficial in some instances, but detrimental in other cases.

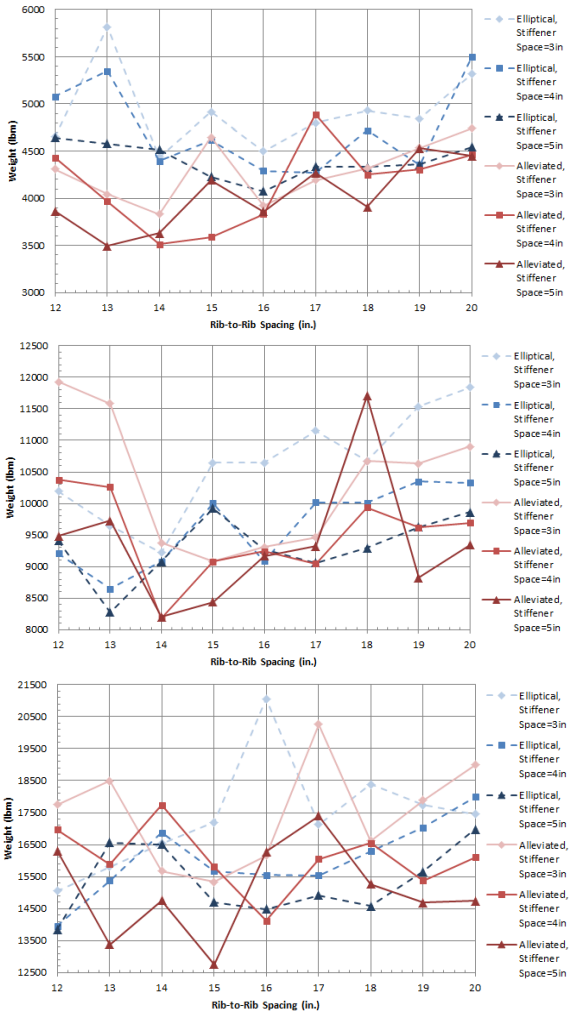

Figure 13. Actual Torque Box Weight Trades. *a)Regional Jet Weights, b)Small Narrow-Body, c)Large Narrow-Body.*

A. Regional Jet Trades

The lightest weight case for the wing with and without active-load-alleviation is displayed below in Table 4. Note the case without active-load-alleviation was achieved by running the structural sizing code with a rib-to-rib spacing of 13 in. and stiffener spacing of 5 in. The best case weight for the weights with active-load-alleviation was run with a rib-to-rib spacing of 16 in. and stiffener spacing of 5 in.

Table 4. Regional Jet, Best Wing Weight Results

	Without Alleviation	With Alleviation	Difference
Actual Torque Box Weight (lbm)	4077.11	3495.47	14.27%
Tensile Torque Box Weight (lbm)	1615.04	1341.10	16.96%
Rib Weight (lbm)	303.38	368.60	-21.50%
Spar Weight (lbm)	241.93	225.81	6.66%
Spar Cover Weight (lbm)	3531.80	2901.06	17.86%

From the high level results of Table 4, it can be seen that ultimately, in the case of an aircraft around 50,000-lbm, active-load-alleviation will produce a 14% reduction in weight of the wing with reflexed ailerons, and a 17% reduction of weight in the non-buckling sized portion of the torque box weight. It is important to remember that this is between the two best weights for the entire trade study for this category. Although their internal structure differs considerably in detail, our optimizer designed structure seems to be able to extract most of the promised weight savings arising from the reduction in root bending moment.

Figure 14 displays the aerodynamic loads and inertial loads in a "lumped mass" form. This "lumped mass" form displays the loads involved in each cell (the number of cells differs between the baseline to active-load-alleviation design because the optimal rib-to-rib spacing is different). The loads include aerodynamic loads (aeroloads), fuel mass, structural mass, and non-structural mass (leading edges, ailerons, actuators, antennae, fuel, hydraulic and electric systems). Recall that the engines are assumed to be located on the fuselage of this aircraft; this is why there is no point at which an engine size load is added. Each cell is roughly the length of the chord, and 1.33 ft wide for Figure 14a and 1.08 ft wide for Figure 14b. In Figure 14a we see an elliptical distribution of aeroloads, as is expected in the non-load alleviated case. For Figure 14b the half span maintains an elliptical behavior until a point between cell 26 and 27, where an inflection occurs in the aeroloads causing a drastic reduction outboard of that point. This affect is attributed to the negative deflection of the ailerons in this region of the wing. Furthermore, the decrease in aeroloads is so drastic that the load empty and full fuel net loads become larger than the aeroloads. Theoretically, this should lead to an opposing moment on the tip, which should be reflected in the stresses.

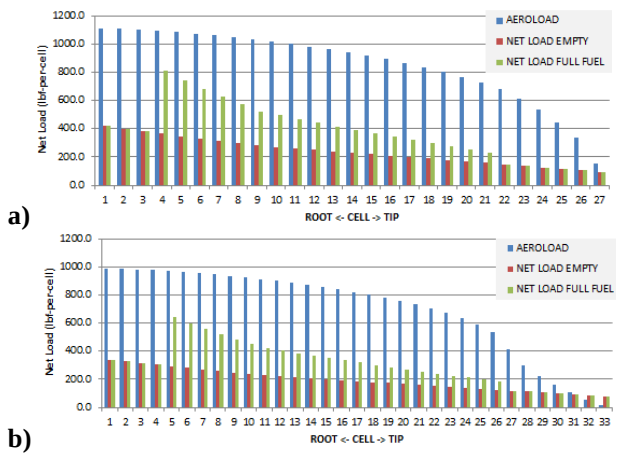

Figure 14. Lumped Load vs Load Cell. *Aerodynamic Loads and inertial loads lumped into cells across half span. a)Without Active-load-alleviation, b)With Active-load-alleviation.*

Figure 15 displays the section *CL* across the half span. The addition of active-load-alleviation creates an inflection in the *CL* curve at the *BL=~27 ft*. Furthermore, active-load-alleviation shifts the maximum *CL* about 8 ft. inboard.

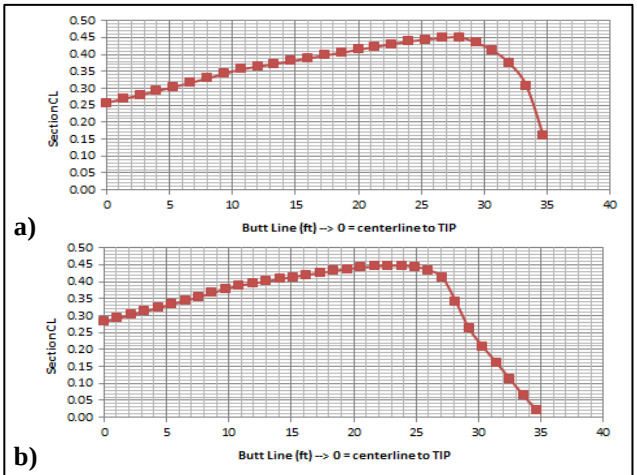

Figure 15. Section CL vs BL. *a)Without Active-load-alleviation, b)With Active-load-alleviation.*

Figures 16 and 17 describe various bending stresses and forces that the wing experiences. A comparison between Figures 16a, 16b and 17a and 17b demonstrates the effects of reshaping the transverse lift distribution on the bending moment. Ultimately both wings must develop the same lift, thus the 1-G shear at the wing root (*BL=0-ft*) is identical between the two wings. However, the reduction in bending torque imposed by the lift distribution is clear. With a small amount of upwards deflection of the ailerons, effectively unloading the wing tips, the root bending torque declines by about 10%. The trends displayed in Figures 16 and 17 are common throughout all aircraft classes examined in this study.

In Figure 18, we see how the optimizer selected design develops a minimum weight compliant design. The optimizer sizes skin thickness, spar cap sizes and stiffener sizes on a "bay-by-bay" basis from wing root to tip. With active-load-alleviation, the lower bending torque leads to a design with significantly different geometry over the inboard half of the semi-span.

In Figure 18a, for the nominal design, we find a design strategy where the skin takes the majority of the load; followed by the stiffeners taking the second largest portion until they reach the tip when the optimizer offloads the weight onto the sparcaps.

In Figure 18b, for the active-load-alleviation design, the optimizer finds weight savings by reconceptualizing the inboard structure. For *BL<16-ft*, the minimum weight solution derives from a structure with thinner skins (see Figures 18a and 18b) that carries more load in the stiffeners and spar caps.

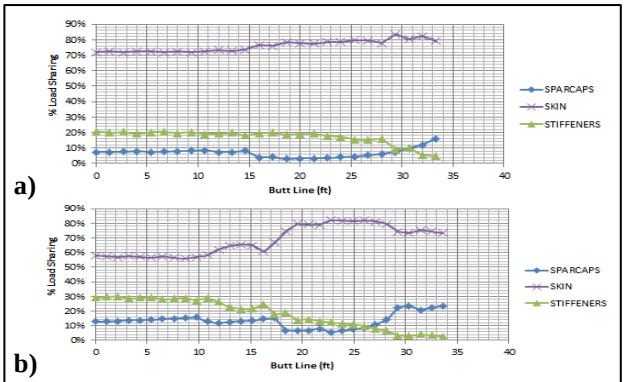

Figure 18. Percent Load Sharing vs BL. *Graph of how the load is shared between spar caps, skin, and stringers on the optimized wing. a)Without Active-load-alleviation, b)With Active-load-alleviation.*

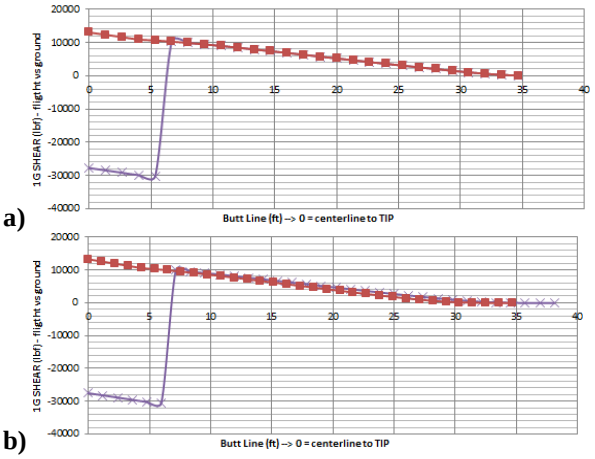

Figure 16. 1-G Shear vs BL. *Shear for Nz=±1 cases, note that purple line is Nz=-1. a)Without Active-load-alleviation, b)With Active-load-alleviation.*

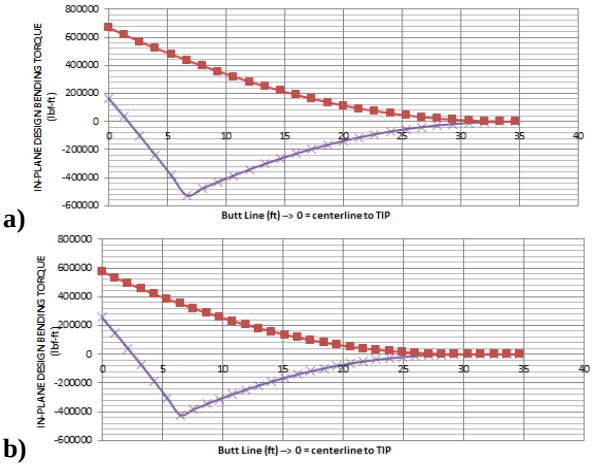

Figure 17. In-Plane Bending Torque vs BL. *Bending Moment for Nz=±1 cases, note that purple line is Nz=-1. a)Without Active-load-alleviation, b)With Active-load-alleviation.*

Figure 19 shows what the optimizer selected as the optimum skin thickness across the half-span of the wing. Notably, we see in 19a, the optimizer selects an elliptical scheme, with a larger root skin thickness of 0.35 inches to safely address the stresses experienced in the non-load-alleviated case. But once load-alleviation is added the optimizer is able to lower the root thickness to 0.25 inches, and have the elliptical trend approach a thinner thickness at a point more inboard. To better understand this behavior it is important to reference Figure 18, which gives some insight into how the distribution of loads change between the two cases, allowing for the more irregular skin thickness distribution.

Figure 20 displays the minimum cover area, which is the area needed to meet the conditions for just the tension loading criteria, and the actual cover area which represents the area needed to meet the conditions for tension, compression, stiffened panel buckling, and local panel buckling criteria. From this information, it is seen that at all points in the wing the other criterion are prevalent enough to require a significant amount of additional area for structural stability (as opposed to structural strength), with the biggest point being at the root. So as a result this is a buckling driven structure, not a strength driven structure.

In Figure 21, we can see more clearly the source of the necessary increase in weight. In all cases, the local panel buckling (that is the buckling of the otherwise unsupported skin between ribs and stiffeners) drives the structural design. However, the lighter weight active-load-alleviation design allows for a structure where the overall stiffened panel buckling criterion rises to the same level of importance as the local buckling criterion. This explains why the optimizer off loads the forces onto the spar caps so drastically (refer back to Figure 17b).

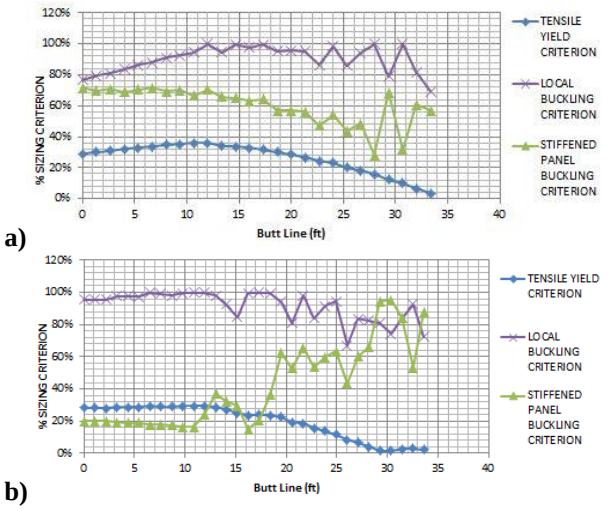

Figure 21. Sizing Criterion vs BL. *Shows which failure criterion is driving the optimizer solution. a)Without Active-load-alleviation, b)With Active-load-alleviation.*

Figure 22 displays the dimensions of the spar caps as a function of span. A comparison between Figures 22a and 22b reveals that the active-load-alleviation case requires that the spar caps maintain a larger width near the root of the wing to deal with the forces involved.

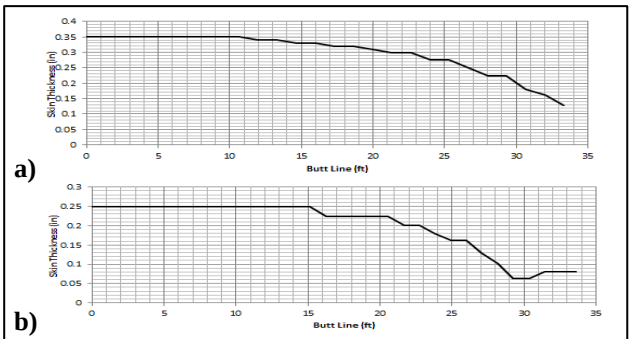

Figure 19. Skin Thickness vs BL. *a)Without Active-load-alleviation, b)With Active-load-alleviation.*

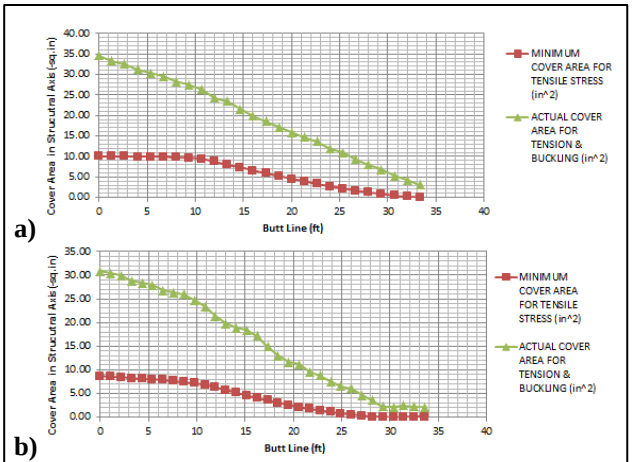

Figure 20. Cover Area in Structural Axis vs BL. *a)Without Active-load-alleviation, b)With Active-load-alleviation.*

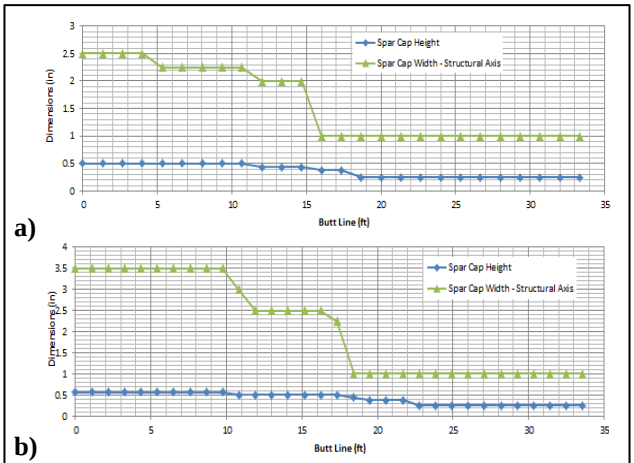

Figure 22. Spar Cap Dimensions vs BL. *Shows change of spar cap dimensions throughout the wing. a)Without Active-load-alleviation, b)With Active-load-alleviation.*

Figures 23 and 24 display the dimensions of and number of stiffeners across the wing. A comparison between the respective plots (Figure 23a and 23b as well as Figure 24 and 24b) plots reveals an interesting result; that active-load-alleviation allows for smaller stiffeners on the outboard portion of the wing.

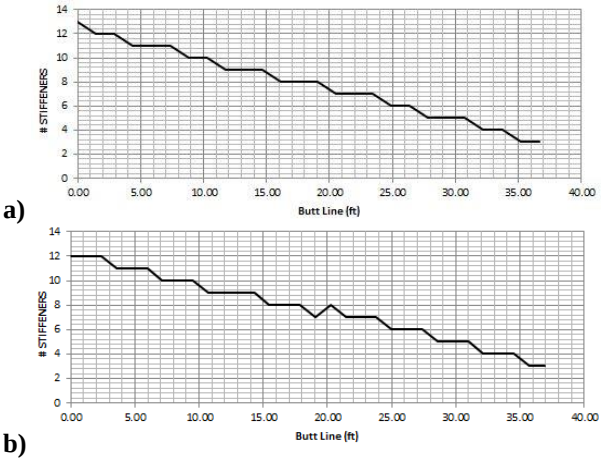

Figure 23. Number of Stiffeners vs BL. *Shows the lumped Aerodynamic Loads and inertial loads. a)Without Active-load-alleviation, b)With Active-load-alleviation.*

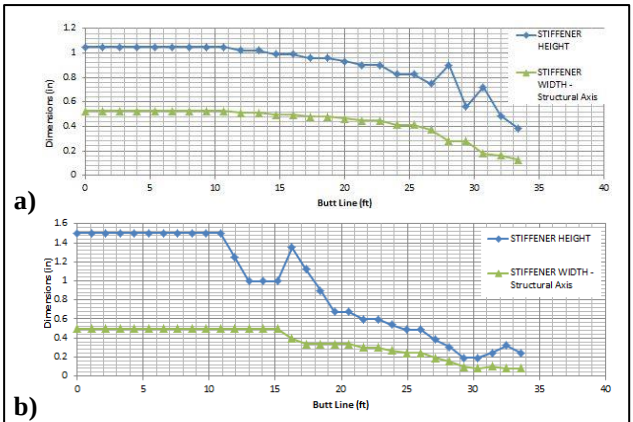

Figure 24. Stiffener Thickness vs BL. *Shows the lumped Aerodynamic Loads and inertial loads. a)Without Active-load-alleviation, b)With Active-load-alleviation.*

B. Small Narrow-Body Airliner

In this section of the paper, we examine a 100,000-lbm class airliner with geometry roughly equivalent to an old Boeing 737-100. The lightest weight case for the wing with and without active-load-alleviation is displayed below in Table 5. The best case weight without active-load-alleviation was found using a rib-to-rib spacing of 13 in. and stiffener spacing of 5 in. The best case weight for the weights with active-load-alleviation was run with a rib-to-rib spacing of 14 in. and stiffener spacing of 4 in.

Table 5. Small Narrow-Body, Best Wing Weight Results

	Without Alleviation	With Alleviation	Difference
Actual Torque Box Weight (lbm)	8275.29	8185.00	1.09%
Tensile Torque Box Weight (lbm)	5046.47	4216.37	16.45%
Rib Weight (lbm)	1222.67	1134.61	7.20%
Spar Weight (lbm)	657.09	608.68	7.37%
Spar Cover Weight (lbm)	6395.54	6441.72	-0.72%

From the top level results shown in the table above it can be seen that active-load-alleviation produces about an overall 1% reduction in weight of the wing with a reflexed aileron. Yet in the tensile portion of the torque box weight there is about a 17% weight reduction. Thus, the "devil is in the details;" while a significant theoretical weight savings is implied, our optimizer cannot find such savings in the buckling dominated structural formulation.

Figure 25 shows how active-load-alleviation impacts the loads in each cell on this wing. We should note that this wing, like the regional jet wing (recall Figure 14), optimizes in a manner where the number of cells differs between the baseline to active-load-alleviation design because the optimal rib-to-rib spacing changes based on the altered spanwise load distribution. Here, the active-load-alleviation design has a wider rib-to-rib spacing than the baseline. To attain the same overall lift with reflexed ailerons requires a stronger aeroload at the root to balance against the greatly reduced aeroload at the tip. As we found on the regional jet case, Figure 25b shows a point near the tip where the net empty weight and net full fuel inertial loads overcome the aeroloads, theoretically creating an opposing moment in the structure.

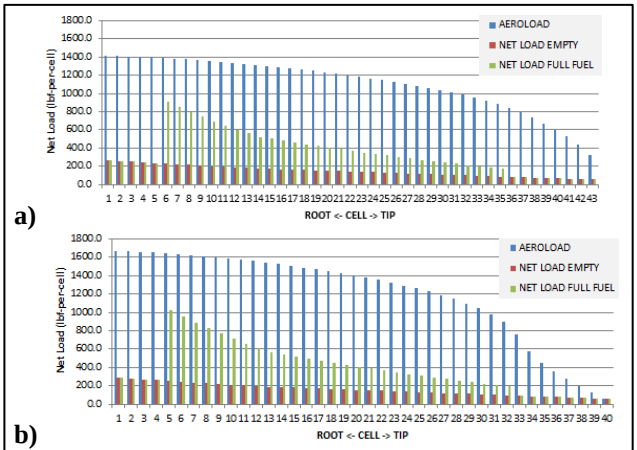

Figure 25. Lumped Load vs Load Cell. *Shows the lumped Aerodynamic Loads and inertial loads. a)Without Active-load-alleviation, b)With Active-load-alleviation.*

Figure 26 highlights the impact of root bending moment relief upon this wing. In Figure 26a we see the root dominated by the stiffened panel buckling criterion, which quickly gives way to the local buckling criterion throughout the rest of the wing. The tensile yield criterion is never active; hence the global wing structure is dominated by some form of buckling challenge (either large stiffened panel or local strip buckling).

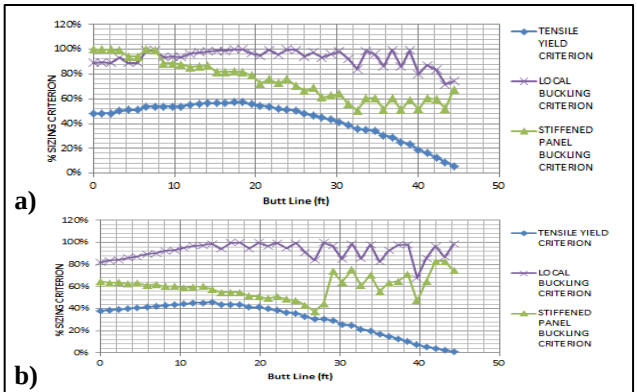

Figure 26. Sizing Criterion vs BL. *a)Without Active-load-alleviation, b)With Active-load-alleviation.*

The addition of active-load-alleviation in 26b creates a very different result, chiefly being the significant reduction of the entire criterion at the root (the optimizer heuristics of having constant physical stiffener spacing and monotonic reductions in skin thickness work against us here). Yet, this wing is a fully local "strip" buckling as opposed to stiffened panel buckling dominated design. In order to extract a greater weight savings, we would have to radically rethink the density of stiffeners in the region of the wing root.

In Figure 27 we once again see that the active-load-alleviation slightly reduces the minimum cover area required to resist the tensile forces. But when all of the buckling characteristics are considered, we find that our optimizer actually builds a lighter wing outboard of BL=+/-15-ft for the active-load-alleviation case and a heavier wing inboard.

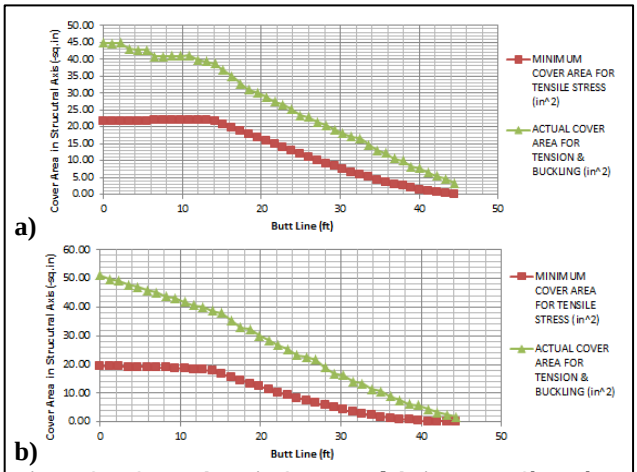

Figure 27. Cover Area in Structural Axis vs BL. *Shows how the load is shared between spar caps, skin and stringers on the optimized wing. a)Without Active-load-alleviation, b)With Active-load-alleviation.*

On the outer wing panels, the optimizer selected thinner wing skins. Across the entire wing, the optimizer selected smaller spar caps. The "wash" in weight was entirely the result of the balance between stiffener size and density. The geometry of this wing,

when coupled to bending torques arising from active-load-alleviation demands a spanwise tailoring of stiffener spacing. With constant stiffener spacing, the optimizer selected thicker stiffeners at the root, but smaller stiffeners at the tip as compared to the baseline design.

C. Large Narrow-Body Airliner

In this section of the paper, we examine a 150,000-lbm class airliner with geometry roughly equivalent to an Airbus 320. The lightest weight case for the wing with and without active-load-alleviation is displayed below in Table 6. Note that the case without active-load-alleviation was designed for a 12 inch rib spacing and 5 inches between stiffeners. Then the case with active-load-alleviation was designed for a 15 inch rib spacing and 5 inch stiffener spacing.

Table 6. Large Narrow-Body, Best Wing Weight Results

	Without Alleviation	With Alleviation	Difference
Actual Torque Box Weight (lbm)	13853.81	12757.07	7.92%
Tensile Torque Box Weight (lbm)	9525.44	7742.57	18.72%
Rib Weight (lbm)	2080.55	1664.66	19.99%
Spar Weight (lbm)	1127.21	1064.45	5.57%
Spar Cover Weight (lbm)	10646.05	10027.97	5.81%

Based on the lightest possible weights for each case it is shown that the active-load-alleviation case will reduce the overall weight of the torque box by about 8%, and astonishingly predicts a 19% of weight savings in the tensile torque box. Here, our optimizer driven design can only realize half of this theoretical weight savings.

In general, we observed similar behavior compared with the other aircraft cases, where the skin carries the majority of the load. However, this geometry was interesting in that the optimizer, when faced with active-load-alleviation actually increases the skin thickness (see Figure 28) and decreased the size of the spar caps (see Figure 29) to find the lightest weight structure.

Without active-load-alleviation, we found the optimizer choosing a structural layout where the design was dominated by the local buckling criterion. When active-load-alleviation is applied, the optimizer chooses a design where the stiffened panel buckling criterion controls the design over the majority of the center span.

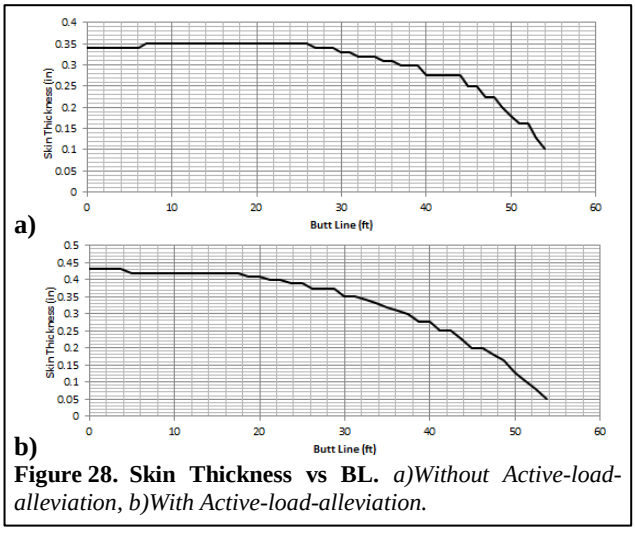

Figure 28. Skin Thickness vs BL. *a)Without Active-load-alleviation, b)With Active-load-alleviation.*

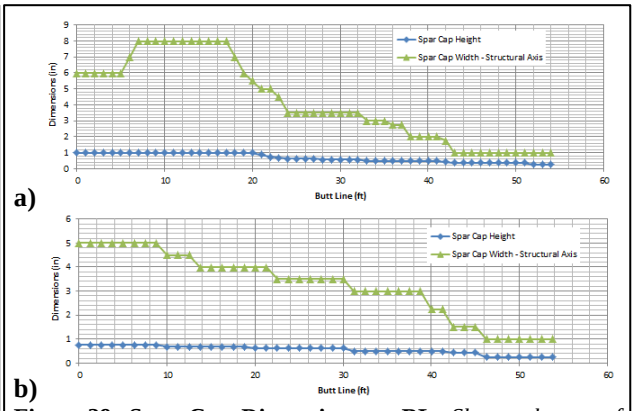

Figure 29. Spar Cap Dimensions vs BL. *Shows change of spar cap dimensions throughout the wing. a)Without Active-load-alleviation, b)With Active-load-alleviation.*

IV. Discussion

One of the common themes across all classes of aircraft examined in this manuscript is seen in the aeroload data, where the maximum section *CL* is shifted inboard of the maximum section *CL* on the elliptical case. Additionally for the 100,000-lbm and 150,000-lbm designs, the aeroloads on the portion inboard of the inflection point see an increase in their loads across that portion of the span, while the 50,000-lbm design sees a slight decrease.

The effects of the changes in the maximum *CL* and the transverse *CL* distribution are also seen in the bending torques; where after the addition of active-load-alleviation, the bending torques measured at the root of the wing see a decrease of about 10% with only a 2.5° symmetric droop in the ailerons. This behavior can be theoretically rationalized through the fact that by reshaping the lift distribution, such that the aeroloads are moved closer to the root, will create a smaller moment arm for those forces to act effectively reducing the bending moment experienced by the wing. Additionally the change in the lift distribution across the wing does not change the *1-G* shear experienced by the wing root; meaning that active-load-alleviation does not appear to influence the shears on the wing.

From the data collected on load sharing in the wing (Figures 18, 21, 26) it is discovered that one of the biggest effects active-load-alleviation has on the wing structure is influencing which elements receive the majority of the load. An interesting result is that the regional jet and small narrow-body cases see a result where the addition of active-load-alleviation causes the load carried by the skin at the root to decrease, and shift more of the load onto the spar caps and stiffeners; with the stiffeners carrying more than the spar caps. Although, for the large narrow-body case the addition of active-load-alleviation actually increases the load carried by the skin, therefore decreasing the amount on the spar caps and stiffeners. But this change has the added benefit of making the stiffeners more consistently carry more of the load than the spar caps.

In all cases examined the tensile yield criterion is reduced by various amounts when active-load-alleviation is applied to the aircraft. The various amounts usually stay around 5-10% reduction. In the regional jet and large narrow-body cases the addition of active-load-alleviation causes a reduction in the local buckling criteria at the root, and an increase in the stiffened panel buckling criteria simultaneously. This behavior is followed by a midspan portion that is dominated by the local buckling criteria and then a spike by the stiffened panel buckling criteria at the tip. The small narrow-body goes against this trend, where the addition of active-load-alleviation not only reduces the local buckling criterion at the root, but also the stiffened panel buckling criterion. This is then followed by a portion where the stiffened panel buckling criterion spikes up (like in the other cases) but instead of reaching above the local buckling criterion, it mirrors the increases and decreases as the tip is approached.

The spar caps dimensions yield a result that active-load-alleviation produces larger spar caps, except on the outboard half of the span where the spar cap is the same area as the non-alleviated case. For both the narrow-body cases the addition of active-load-alleviation allows for spar caps with a smaller area that is once again matched at the tip.

For the regional jet and small narrow-body cases the addition of active-load-alleviation produces a case where the skin across the wing can be thinner than its non-alleviated counterpart. But in the large narrow-body case, the root ends up requiring more thickness, and the tip is allowed to ultimately have a thinner skin than the counterpart.

For the stiffeners, active-load-alleviation creates an instance in the regional jet where the root has fewer stiffeners, but they are larger in area, and then transitions to having about the same number of stiffeners at the tip but with smaller areas. In the case of the small narrow-body, active-load-alleviation produces a situation where there are more stiffeners across the wing, but they are bigger than their counterpart at the root and smaller at the tip. In the large narrow-body, active-load-alleviation results in roughly the same number of stiffeners but that have a smaller area across the entire span.

An additional output of the structural sizing tool allows us to examine the weight of a few key components to the structural design of the wing. The component that consistently produces the biggest weight change across all

categories of aircraft examined is the weight of the ribs. For the regional jet the rib weight actually sees a 22% increase in weight when active-load-alleviation is added; while the biggest weight reduction is seen by the large narrow-body which sees a 20% reduction, and small narrow-body aircraft sees a more modest 7% weight reduction. These drastic changes in weight of components can be better understood with reference to the sizing criteria plots, Figure 17 for the regional jet, and Figure 21 for the small narrow-body. For the regional jet we see that the addition of active-load-alleviation forces the local buckling criterion to become the dominant criteria throughout almost all the wing, especially at the root. For the small narrow-body we see a similar behavior, where the local buckling criterion becomes dominant after active-load-alleviation is added, but the stiffened panel buckling still stays at the level of notable importance. This difference in how active-load-alleviation affects the distribution of loads would lead the optimizer to make major changes to the design, especially near the root. In the case of the regional jet, to address the newly increased importance of local buckling; while with the small-narrow body the optimizer can actually decrease the sizing of components near the root

All these factors ultimately produce a consistent result of a weight reduction in every wing examined. The best total reduction is seen in the regional jet with a 14% weight reduction in the total torque box, and a 17% reduction the tensile torque box. The small narrow-body sees a small 1% weight reduction between the total torque box weights, but once again a 17% reduction in the tensile torque box. The large narrow body sees a total torque box weight reduction of 8% and a tensile torque box reduction of 20%.

V. Conclusions

The results presented here show that active-load-alleviation through symmetric reflexed ailerons produces complicated and multifactor effects in the fundamental design of the wing. Such technology needs to be incorporated at the outset of design; its presence alters the optimal layout of ribs and stiffeners. This is seen through the fact that the first and second best overall wing weight reductions are seen in the lightest (regional jet) and heaviest aircraft (large narrow-body) examined by this paper, 14% and 8% respectively. While the small narrow-body saw a small 1% weight reduction. Based on the results in this paper, this variability in results can be attributed to how the change in loads affects the internal structure of the wing, and whether it lines up in the perfect way to yield significant gains.

We conclude that, based on the wide range of variation experienced by certain components within the structure of the aircraft, that the degree of effects of active-load-alleviation are dependent on the size of the aircraft. Because as was seen in the regional jet, the addition of active-load-alleviation drastically changed the chief concerns of the optimizer near the root from a mixture of local buckling criterion and stiffened panel buckling criterion to almost solely local buckling criterion. While for the narrow-body, it does once again make the local buckling criterion more important at the root, but at the same time actually reducing it from about 95% to about 80%. Additionally, active-load-alleviation does not force the other criterion to such a low level that they are largely unimportant, which would vastly change the solution found by the optimizer.

Acknowledgments

This paper derives from unsponsored research work Mr. Allyn performed in partial fulfillment of degree requirements for obtaining his M.S. in Aerospace Engineering from Arizona State University. All analysis was performed at Arizona State University.

References

[1] Disney, T.E., "C-5A Active-load-alleviation System, *Journal of Spacecraft*, Vol. 14, No. 2, 81-86, 1977.
[2] Xu, J., and Kroo, I., "Aircraft Design with Active-load-alleviation and Natural Laminar Flow", *Journal of Aircraft*, Vol. 51, No. 5, 1532-1545, Sept.-Oct. 2014.
[3] Miranda, L. R., Baker, R. D., and Elliott, W. M., "A Generalized Vortex Lattice Method for Subsonic and Supersonic Flow," NASA CR 2875, 1977.

[4] Takahashi, T.T. and Lemonds, T., "Prediction of Wing Structural Mass for Transport Category Aircraft Conceptual Design," AIAA 2015-3374, 2015.
[5] Takahashi, T.T. and Lemonds, T., "Transport Category Wing Weight Estimation Using A Optimizing Beam-Element Structural Formulation," AIAA 2015-1898, 2015
[6] MIL HDBK 5-J
[7] Niu, M. C-Y, *Airframe Structural Design: Practical Design Information and Data on Aircraft Structures, 2nd Edition ,* Adaso/Adastra Engineering Center; 2nd edition